RESEARCH ARTICLE
doi: 10.2306/scienceasia1513-1874.2021.028

ScienceAsia 47 (2021): **241–250**

A diffusion model of ^{18}F-FDOPA in the diagnosis of Parkinson's disease and its numerical simulation

Printaporn Sanguansuttigul[a], **Teerapol Saleewong**[a,b,*], **Kitiwat Khamwan**[c], **Saknan Bongsebandhu-phubhakdi**[d]

[a] Department of Mathematics, Faculty of Science, King Mongkut's University of Technology Thonburi, Bangkok 10140 Thailand
[b] Theoretical and Computational Science Center (TaCS), Faculty of Science, King Mongkut's University of Technology Thonburi, Bangkok 10140 Thailand
[c] Department of Radiology, Faculty of Medicine, Chulalongkorn University, Bangkok 10330 Thailand
[d] Department of Physiology, Faculty of Medicine, Chulalongkorn University, Bangkok 10330 Thailand

*Corresponding author, e-mail: Teerapol.sal@kmutt.ac.th

Received 14 Oct 2020
Accepted 20 Dec 2020

ABSTRACT: This research aims to study the concentration change of the radioactive substance ^{18}F-FDOPA, which is the key method to diagnose the Parkinson's disease (PD), using the diffusion equation. The model aims at approximating the concentration over the brain region called striatum. From the PET/CT images of the whole brain, the striatum site was segmented using the Otsu's method. The region obtained from the segmentation is then used as the domain for our diffusion model. We then adopt the ADI method of [17] to the non-rectangular domain. The diffusion parameters are improved by mean of the pattern search method to best fit with the true data. After comparing the numerical solution at the final timestep with the actual data, we can finally be positive that our diffusion model is consistent with the actual data and lead to the same diagnosis of the Parkinson's disease.

KEYWORDS: diffusion model, Parkinson's disease, ADI method, image segmentation

MSC2010: 65M06 65M22

INTRODUCTION

Pakinson's disease (PD) is caused by a disorder of nerve cells in a brain area called the substantia nigra which controls body movement. Nerve cells in this part are responsible for producing an important chemical called dopamine. Loss of dopaminergic innervation to the striatum (and basal ganglia) results in PD. The striatum, consisting of putamen and caudate nucleus [1–4], is a hub in the basal ganglia circuitry controlling goal directed actions and habits, hence is an important part to diagnose the PD patients. PD affects about 1–3% of the global population aged over 60 years [5]. We suspect a patient to have a PD symtoms after they were diagnosed to lose approximately 50–60% of the dopamine neurons. Dopamine is a chemical messenger that carries signals between brain and other cells, and the signal of dopamine released in the striatum [6, 7]. Patients with Parkinson's disease can be diagnosed using Diagnostic Radiology [8]. In this research, we want to study the radioactivity of ^{18}F-FDOPA, which is related to the dopamine *in vivo* [9, 10].

The patient will be injected ^{18}F-FDOPA and it shows the intensity of the dopamine remaining in brain [11]. Positron Emission Tomography - Computed Tomography (PET/CT) scan is a type of nuclear medicine imaging and the most commonly used for radiotracer because PET scan produces the intensity of the radioactivity and CT scan produces a detailed image of structures inside the body. PET/CT scan combines PET and CT imaging and then provides a clear picture of what is happening in the body. The concentration of ^{18}F-FDOPA is detected by PET/CT scan 90 minutes after injection.

The patient's data is recorded from King Chulalongkorn Memorial Hospital with a PET/CT scan. The PET/CT imaging can help physicians to accurately diagnose many diseases early on when treatment is more likely to be effective. For example, the grayscale image of PET/CT scan as shown in Fig. 1 illustrate the intensive of the radioactivity. The idea to set up a mathematical model for approximating the concentration of ^{18}F-FDOPA is described by Fick's law, which is a simple description of the

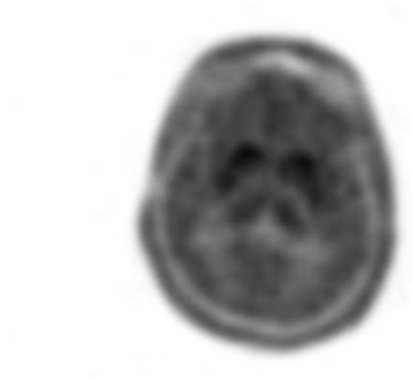

Fig. 1: The grayscale image shows the concentration of ^{18}F-FDOPA.

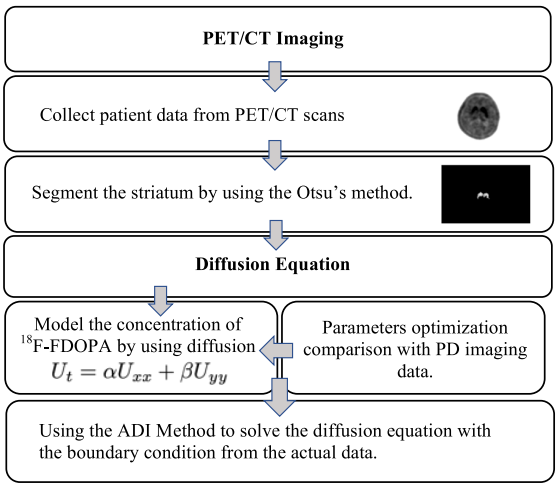

Fig. 2: Conceptual framework of methodology.

flux of chemical to approximate the concentration of chemical which diffuse through a unit area during a unit time interval [12, 13]. The concentration is collected by using the thresholding by Otsu's technique [14].

In this research, we study the behaviour of ^{18}F-FDOPA to gain a better understanding of the diffusion mechanism of drug-disease or the concentration of radiotracers, which is related to the disease and treatment. It also optimizes clinical trials through modeling and clinical trial simulations in the future. The main idea of this research is to apply a diffusion model by Fick's law to approximate the concentration of ^{18}F-FDOPA, which is stored in striatum at each time t. This research should yield a new knowledge that can be applied to Parkinson clinical diagnosis and treatment. The main results of this paper concerns with the following advantages. (1) The numerical method of this paper is based on the segmentation technique which allows us to neglect the unrelated effects outside the ROIs. (2) The simulation of this paper can be applied in case of missing or corrupted PET/CT scans. (3) The time increment in the simulation can be refined to interpolate the concentration of the radiopharmaceutical in the missing time. In addition to these benefits, the proposed method can hopefully be extended to study the diffusion behavior of other radioactivity substances, for example ^{18}F-FDG which is commonly used in oncology.

METHODOLOGY

In this paper, we study the concentration in the striatum by firstly start collecting the actual data using PET/CT imaging to observe brain activities of Parkinson's patients. After the data is collected, we perform the brain area segmentation to the

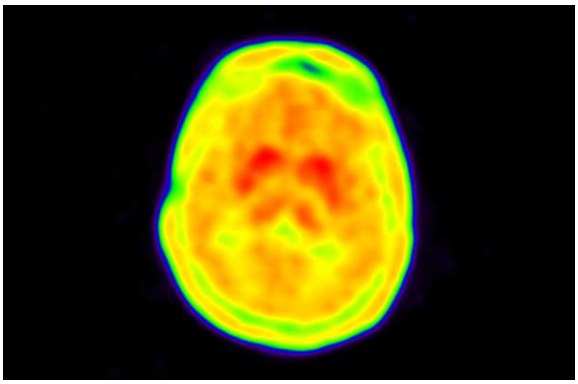

Fig. 3: The example of PET/CT imaging after colours the image.

striatum by using the Otsu's thresholding technique to highlight the brain site where the ^{18}F-FDOPA uptake takes place. To understand the ^{18}F-FDOPA uptake and describe the behaviour of this radioactivity, we use the idea of Fick's law [13], which is the most commonly used method for describing the diffusion of radioactive tracers in tissue. After that Alternating Direction Implicit (ADI) method is used to describe the ^{18}F-FDOPA uptake, see Fig. 2.

Data collection

Data collection is recorded from King Chulalongkorn Memorial Hospital. The patients will be scanned with PET/CT once every 5 min for 90 min records the grayscale images as shown in Fig. 1, then it is easier if we visualize the image in colors as shown in Fig. 3. In this section, we explain the method of collecting the data by using the thresholding technique from the computer vision

theory. Thresholding is a process in which a group of thresholds is optimally chosen under a given criteria, which assign each pixel into a class. In this paper, we use the Otsu's technique, which is one of the most successful methods for image thresholding due to its simple and inexpensive calculation. Otsu's technique is an automatic threshold selection region based segmentation method. The useful data we adopted in this paper is extracted from the area of the striatum, which is related to the diagnosis of PD.

From Fig. 3 our Region of Interests (ROIs), namely the striatum (red area), where the radioactivity of ^{18}F-FDOPA is intensely stored, is detected by applying the Otsu's technique. In this work, our data is collected from PET/CT imaging as can be seen from Fig. 3. We use thresholding by Otsu's technique to collect the area of striatum in order to fix the boundary condition used in our proposed mathematical model. In terms of mathematics, if the radioactivity at both sides of striatum cannot be computed, then we need to separate the side to approximate the concentration. After the radioactivity at both sides of the striatum were collected using the thresholding technique described above, we use the techniques of mathematical modelling and numerical methods, namely, the ADI method, to approximate the concentration ^{18}F-FDOPA at each position x, y and time t.

Fig. 3 shows the concentration level of 18F-FDOPA in the whole brain. Our ROI (striatum area) should be considered separately in the left and right sides, since the concentration of each side gives a different sign for diagnosis of the Parkinson's disease. In this paper, we select the three patients, who were diagnosed with different brain disorders as our sample cases. This will ensure our method is capable of explaining the diffusion of ^{18}F-FDOPA in each situation.

Otsu's technique

In this section, we explain the method of collecting the data by using the thresholding technique from the computer vision theory. Thresholding is a process in which a group of thresholds is optimally chosen under a given criteria, which assign each pixel into a class. In this topic, we use the Otsu's Algorithm, which is widely considered as one of the most successful methods for image thresholding due to its simplicity and inexpensive calculation. Otsu's technique is an automatic threshold selection region based segmentation method. The useful data we adopted in this paper is extracted from the area of the striatum, which is related to the diagnosis of PD. It was developed in [16] based on the maximisation of the between-class variance:

$$\underset{(th_0,\ldots,th_n)\in \mathrm{TH}}{\operatorname{argmax}} \sum_{i,j\in\{0,1,2\}} \omega_i \omega_j (\sigma_i - \sigma_j)^2, \qquad (1)$$

where TH is a class of all set of threshold. Here, i and j index the intensity classes, and ω_i and σ_i are the probability of occurrence and the mean of a class, respectively. Such values are obtained as:

$$\omega_i = \sum_{j=th_{i-1}+1}^{th_i} p_j \quad \text{and} \quad \sigma_i = \sum_{j=th_{i-1}+1}^{th_i} \frac{p_i}{\omega_i} j,$$

where p_j denotes the probability distribution of pixel. Applying the Otsu's technique to our PET/CT data, we obtain the ^{18}F-FDOPA concentration in the ROI. After we collect the area of striatum, the next step is to define the domain and the boundary condition that will be used in the diffusion equation model for approximating the concentration of the radioactivity.

Diffusion equation

The diffusion equation was designed by using a mathematical model to explain diffusion of ^{18}F-FDOPA from the PET/CT imaging. In this work, we emphasize that the concentration of ^{18}F-FDOPA, which diffuses through brain and the striatum will absorb this chemical, while using PET/CT images in the axial plane shown in Fig. 3.

Let Ω be the domain of our ROIs and let $U(x, y, t)$ be the concentration of ^{18}F-FDOPA at each position x, y and time t. Thus, the concentration of ^{18}F-FDOPA can be explained by Fick's laws of diffusion derived by Adolf Fick [13]. Here, we use the diffusion equation in 2D as follows:

$$U_t = \alpha U_{xx} + \beta U_{yy}, \qquad (2)$$

where $\alpha, \beta \neq 0$ are the diffusion coefficient in the direction of x and y, respectively. Since our ROI is a non-rectangular domain, we will define the boundary conditions and choose the method to match our domain using the idea from Steven Wray [17].

2D ADI method for non-rectangular domain

We select the Alternating Direction Implicit (ADI), which suits to our data. The ADI method is an iterative method used to solve tri-diagonal matrix equations. It is a well-known method for solving the large matrix equations [18] and can also be used to numerically solve parabolic and elliptic partial differential equations. In addition, it is a classic

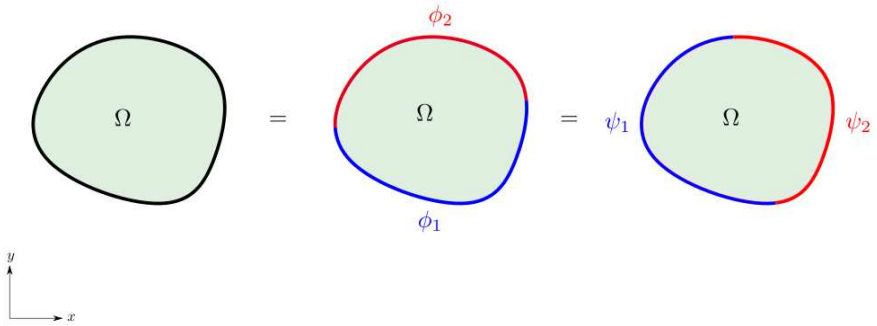

Fig. 4: A domain satisfies the two-part of function.

method used for modeling heat conduction and solving the diffusion equation in two or more dimensions [19]. Our ROI is obviously non-rectangular as one may recall from Fig. 3. This non-rectangular shape forces us to adopt a numerical method that is applicable to such region [17]. In this research, we apply the 2D ADI method for non-rectangular domains to compute the concentration of radioactivity stored at the striatum. Note that the ADI method is known for its stability and an inexpensive computational cost at each step.

We now briefly recall the 2D ADI method for non-rectangular domains firstly proposed in [17]. Let $\Omega \subseteq \mathbb{R}^2$ be a domain that satisfies the two-part definition,

$$\begin{aligned}\Omega &= \{(x,y)\,|\,A<x<B, \phi_1(x)<y<\phi_2(x)\}\\ &= \{(x,y)\,|\,C<y<D, \psi_1(y)<x<\psi_2(y)\},\end{aligned} \quad (3)$$

where A, B are real numbers with $A<B$, and C, D are real numbers with $C<D$ as shown in Fig. 4. Let the step sizes

$$\Delta_x = \frac{B-A}{N} \quad \text{and} \quad \Delta_y = \frac{D-C}{N}$$

be defined by a given number of steps N. Then, we define an array of grid points (x_i, y_j) over the rectangular domain $[A,B]\times[C,D]$ containing Ω, where

$$x_i = A + i\Delta_x, \qquad i = 0,1,\ldots,N$$

and

$$y_j = C + i\Delta_y, \qquad j = 0,1,\ldots,N.$$

Furthermore, the time step size is given by $\tau = \frac{T}{M}$. There are $M+1$ evenly spaced time values in total.

Suppose that the initial conditions are given by

$$u(x,y,0) = h_1(x,y), \quad (x,y)\in\overline{\Omega} \quad (4)$$

and the Dirichlet boundary conditions are given by

$$u(x,y,t) = h_2(x,y,t),\ (x,y)\in\partial\Omega,\ t\in[0,T]. \quad (5)$$

So, we used the ADI Method for approximating the concentration of the radioactivity at position x, y and time t. The ADI Method was adapted from the Crank-Nicolson Method [20], which exploits the second-order central difference at position x and y as follow,

$$\begin{aligned}\delta_x^2 U_{i,j}^m &= \frac{U_{i-1,j}^m - 2U_{i,j}^m + U_{i+1,j}^m}{\Delta_x^2}\\ \delta_y^2 U_{i,j}^m &= \frac{U_{i,j-1}^m - 2U_{i,j}^m + U_{i,j+1}^m}{\Delta_y^2},\end{aligned} \quad (6)$$

for $i,j = 1,\ldots,N-1$ and $m = 0,1,\ldots,M$, where $U_{i,j}^M$ represents $U(x_i, y_i, t_M)$.

The Crank-Nicolson method is the traditional method for solving the diffusion equation numerically, but its expensive computation cost is the main disadvantage which encouraged us to find cheaper alternatives. In 1955, Peaceman and Rachford [19] introduced a numerical method for diffusion equation problem known as the ADI Method. One big advantage of the ADI method is that the equations to be solved in each step have a simpler structure and can be solved efficiently with a tridiagonal matrix algorithm. The idea behind this method is to split time into two fractional time steps, one with the x-derivative and the other one with the y-derivative, both taken implicitly, and combine them with the previous method of Crank-Nicolson method

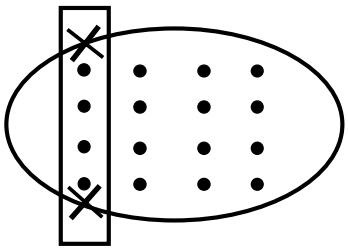

Fig. 5: A nonempty column showing interior points and boundary points.

as follows:

$$V_{i,j}^m = (1+\frac{\beta\tau}{2}\delta_y^2)U_{i,j}^m \quad \text{Step1}$$

$$(1-\frac{\alpha\tau}{2}\delta_x^2)U_{i,j}^{m+\frac{1}{2}} = V_{i,j}^m \quad \text{Step2} \quad (7)$$

$$(1-\frac{\beta\tau}{2}\delta_y^2)U_{i,j}^{m+1} = 2U_{i,j}^{m+\frac{1}{2}} + V_{i,j}^m \quad \text{Step3}$$

where these formulas are applied at all interior points of Ω.

Grid meshing (non-rectangular domain)

In this section , we will restrict our consideration to the gridpoints which lie inside Ω and generate the boundary points at each rows and columns (Fig. 5).

Consider the gridpoints at column i. Let $j_{min(i)}$ and $j_{max(i)}$ be the smallest j and the largest j, respectively, such that (x_i,y_j) is the interior point of domain Ω_N. The boundary points for column i are the points where the vertical line intersects the boundary curves ϕ_1 and ϕ_2.

To describe these points of intersection, define the constants for the lower boundary curves and upper boundary curves as

$$\phi_{(i,l)} = \phi_1 \quad \text{and} \quad \phi_{(i,u)} = \phi_2.$$

Define $U_{i,l}^{\prime m}$ as the boundary value of the solution $U(x_i,y_j,t_m)$ at the lower boundary and $U_{i,u}^{\prime m}$ for the upper boundary as follows:

$$U_{i,l}^{\prime m} = g_2(x_i,\phi_{i,l}) \quad \text{and} \quad U_{i,u}^{\prime m} = g_2(x_i,\phi_{i,u}).$$

Similar to the gridpoints at row j, let $i_{\min(j)}$ and $i_{\max(j)}$ be the smallest i and the largest i, respectively, such that (x_i,y_j) is an interior point. The boundary points for row j are the points where the horizon line intersects the boundary curves ψ_1 and ψ_2. To describe these points of intersection, define the constants for the lower boundary curves and upper boundary curves as

$$\psi_{(j,l)} = \psi_1 \quad \text{and} \quad \psi_{(j,u)} = \psi_2.$$

Also define $U_{j,l}^{\prime\prime m}$ as the boundary value of the solution $U(x_i,y_j,t_m)$ at the lower boundary and $U_{j,u}^{\prime\prime m}$ for the upper boundary as follows:

$$U_{j,l}^{\prime\prime m} = g_2(y_j,\phi_{j,l}) \quad \text{and} \quad U_{j,u}^{\prime\prime m} = g_2(y_j,\phi_{j,u}).$$

Computation of 2D ADI method for non-rectangular domain

Step 1: Recall our difference quotient (7) on irregular grids at step 1 of the ADI method. To implement this step, we may consider the following three possible cases.

(i) If $j_{\max(i)} = j_{\min(i)}$, the column i contains only a single interior point, so this point must be the constant:

$$V_{i,j}^m = U_{i,j}^m + \frac{\beta\tau}{2\Delta_y^2}\left(U_{i,u}^{\prime m} - 2U_{i,j}^m + U_{i,l}^{\prime m}\right) \quad (8)$$

(ii) If $j_{\max(i)} \neq j_{\min(i)}$, the column i contains two or more interior points, then the difference quotient must be matrix-vector equations as following:

$$\mathbf{V}_{i,\cdot}^m = \left(I - B^{(i)}\right)\mathbf{U}_{i,\cdot}^m + \begin{bmatrix} \frac{\beta\tau}{2\Delta_y^2}U_{i,l}^{\prime m} \\ 0 \\ \vdots \\ 0 \\ \frac{\beta\tau}{2\Delta_y^2}U_{i,u}^{\prime m} \end{bmatrix}_{N-1}, \quad (9)$$

where $B^{(i)}$ is the $(N-1)\times(N-1)$ tridiagonal matrix

$$B^{(i)} = \frac{\beta\tau}{2\Delta_y^2}\begin{bmatrix} 2 & -1 & & & \\ -1 & 2 & -1 & & \\ & -1 & \ddots & \ddots & \\ & & \ddots & 2 & -1 \\ & & & -1 & 2 \end{bmatrix},$$

and

$$\mathbf{U}_{i,\cdot}^m = \begin{bmatrix} U_{i,j_{\min(i)}}^m \\ U_{i,j_{\min(i)}+1}^m \\ U_{i,j_{\min(i)}+2}^m \\ \vdots \\ U_{i,j_{\max(i)}}^m \end{bmatrix}, \quad \mathbf{V}_{i,\cdot}^m = \begin{bmatrix} V_{i,j_{\min(i)}}^m \\ V_{i,j_{\min(i)}+1}^m \\ V_{i,j_{\min(i)}+2}^m \\ \vdots \\ V_{i,j_{\max(i)}}^m \end{bmatrix}$$

for $i = 0,1,\ldots,N$ where column i is nonempty.

(iii) If the column i contains interior points but do not lie next to the boundary in the y-direction,

so the difference quotient is basically the central difference:

$$\delta_y^2 U_{i,j}^m = \frac{U_{i,j-1}^m - 2U_{i,j}^m + U_{i,j+1}^m}{\Delta_y^2}, \tag{10}$$

for $i,j = 1,\ldots,N-1$ and $m = 0,1,\ldots,M$.

Step 2: Moving to step 2 of ADI method, which needs to be implicitly considered at row j. Similarly to the previous step, the computation can be separated in three cases:

(i) If $i_{\max(j)} = i_{\min(j)}$, the row j contains only a single interior point so this point must be the constant:

$$U_{i,j}^{m+\frac{1}{2}} - \frac{\alpha\tau}{2\Delta_x^2}\left(U_{j,u}^{\prime\prime m+\frac{1}{2}} - 2U_{i,j}^{m+\frac{1}{2}} + U_{j,l}^{\prime\prime m+\frac{1}{2}}\right) = V_{i,j}^m, \tag{11}$$

which can be rearranged to get

$$\left(1+\frac{\alpha\tau}{\Delta_x^2}\right)U_{i,j}^{m+\frac{1}{2}} = V_{i,j}^m + \frac{\alpha\tau}{2\Delta_x^2}\left(U_{j,u}^{\prime\prime m+\frac{1}{2}} + U_{j,l}^{\prime\prime m+\frac{1}{2}}\right). \tag{12}$$

Note that (12) is a formula for $U_{i,j}^{m+\frac{1}{2}}$.

(ii) If $i_{\max(j)} \neq i_{\min(j)}$, the row j contains two or more interior points. Then we get a system of equations which can be rearranged to get a formula for $U_{i,j}^{m+\frac{1}{2}}$ as matrix-vector equations:

$$(I + C^{(j)})\mathbf{U}_{\cdot,j}^{m+\frac{1}{2}} = \mathbf{V}_{\cdot,j}^m + \begin{bmatrix} \frac{\alpha\tau}{2\Delta_x^2} U_{j,l}^{\prime\prime m+\frac{1}{2}} \\ 0 \\ \vdots \\ 0 \\ \frac{\alpha\tau}{2\Delta_x^2} {}^{\prime\prime m+\frac{1}{2}}_{j,u} \end{bmatrix}, \tag{13}$$

where $C^{(j)}$ is the $(N-1)\times(N-1)$ tridiagonal matrix

$$C^{(j)} = \frac{\alpha\tau}{2\Delta_x^2}\begin{bmatrix} 2 & -1 & & & \\ -1 & 2 & -1 & & \\ & -1 & \ddots & \ddots & \\ & & \ddots & 2 & -1 \\ & & & -1 & 2 \end{bmatrix}$$

and

$$\mathbf{U}_{\cdot,j}^{m+\frac{1}{2}} = \begin{bmatrix} U_{i_{\min(j)},j}^{m+\frac{1}{2}} \\ U_{i_{\min(j)}+1,j}^{m+\frac{1}{2}} \\ U_{i_{\min(j)}+2,j}^{m+\frac{1}{2}} \\ \vdots \\ U_{i_{\max(j)},j}^{m+\frac{1}{2}} \end{bmatrix}$$

for all $j = 0,1,\ldots,N$ such that row j contains more than one interior grid point.

(iii) If the row j contains interior points but do not lie next to the boundary in the x-direction, so the difference quotient is basically the central difference:

$$\delta_x^2 U_{i,j}^m = \frac{U_{i-1,j}^m - 2U_{i,j}^m + U_{i+1,j}^m}{\Delta_x^2} \tag{14}$$

for $i,j = 1,\ldots,N-1$ and $m = 0,1,\ldots,M$.

Step 3: Lastly, the idea of step 3 is the same as steps 1 and 2. At the column i, there are also three possible cases:

(i) If $j_{\max(i)} = j_{\min(i)}$, the column i contains only a single interior point, so this point must be the constant:

$$U_{i,j}^{m+1} - \frac{\beta\tau}{2\Delta_y^2}\left(U_{i,u}^{\prime m+1} - 2U_{i,j}^{m+1} + U_{i,l}^{\prime m+1}\right) = 2U_{i,j}^{m+\frac{1}{2}} + V_{i,j}^m, \tag{15}$$

which can be rearranged to get

$$\left(1+\frac{\beta\tau}{\Delta_y^2}\right)U_{i,j}^{m+1} = 2U_{i,j}^{m+\frac{1}{2}} + V_{i,j}^m + \frac{\beta\tau}{2\Delta_y^2}\left(U_{i,u}^{\prime m+1} + U_{i,l}^{\prime m+1}\right). \tag{16}$$

Note that (16) is a formula for $U_{i,j}^{m+1}$.

(ii) If $j_{\max(i)} \neq j_{\min(i)}$, column i contains two or more interior points, then we get a matrix-vector equations which can be rearranged to get an formula for $U_{i,j}^{m+1}$ as follows:

$$(I+B^{(i)})\mathbf{U}_{i,\cdot}^{m+1} = 2\mathbf{U}_{i,\cdot}^{m+\frac{1}{2}} + \mathbf{V}_{i,\cdot}^m + \begin{bmatrix} \frac{\beta\tau}{2\Delta_y^2} U_{i,l}^{\prime m+1} \\ 0 \\ \vdots \\ 0 \\ \frac{\beta\tau}{2\Delta_y^2} U_{i,u}^{\prime m+1} \end{bmatrix}, \tag{17}$$

where

$$\mathbf{U}_{i,\cdot}^{m+1} = \begin{bmatrix} U_{i,j_{\min(i)}}^{m+1} \\ U_{i,j_{\min(i)}+1}^{m+1} \\ U_{i,j_{\min(i)}+2}^{m+1} \\ \vdots \\ U_{i,j_{\max(i)}}^{m+1} \end{bmatrix}.$$

This is an equation to be evaluated for each $i = 1,\ldots,N-1$.

(iii) If column i contains interior points but do not lie next to the boundary in the y-direction, so the difference quotient is basically the central difference:

$$\delta_y^2 U_{i,j}^m = \frac{U_{i,j-1}^m - 2U_{i,j}^m + U_{i,j+1}^m}{\Delta_y^2},$$

Table 1: The choice of parameters is chosen to match the patient's data by the pattern search method.

Patient	Left-hand side		Right-hand side	
	α	β	α	β
1	−0.500	−1.000	−0.75	−3.000
2	−0.375	−0.500	0.75	1.000
3	−0.500	1.000	−3.00	−1.000

The unit of α and β is min^{-1}.

for $i, j = 1, \ldots, N-1$ and $m = 0, 1, \ldots, M$.

Our ROI (striatum area) should be considered separately in the left and right sides, since the concentration of each side gives a different sign for diagnosis of the Parkinson's disease.

Model evaluation

In this research, the difference of exact concentration values and the modelled values were calculated over all internal grid points, that is:

$$e_{L^2} = \left\{ \sum_{(x_i, y_j \in \Omega_N)} \Delta_x \Delta_y \left(U_{i,j}^M - u(x_i, y_j, t_M) \right)^2 \right\}^{\frac{1}{2}}, \quad (18)$$

where $U_{i,j}^M$ is the approximate concentration of radioactivity, $u(x_i, y_j, t_M)$ is the actual concentration, Δ_x and Δ_y are spacing in the x- and y-directions, respectively.

RESULTS

In this research, we examine the diffusion behavior of ^{18}F-FDOPA and compare the modelled result with the actual data from three patients. Recall that all three patients were diagnosed with different brain disorders. The diffusion equation (2) is used to describe the concentration of the pharmaceutical radioactivity. Then the pattern search method [21, 22] is adopted to optimize the parameters α and β. The parameters α and β adapt to the true diffusion in the x- and y-directions, respectively. So this method gives the parameter of α and β as shown in Table 1.

Segmentation

The pixel area of the striatum can be extracted from PET/CT images using Otsu's segmentation technique. The pixel accuracy of Otsu's method is then validated by the dice score, which is calculated by doubling the area of the overlapping part divided by the area of the union. The dice score is often used to quantify the performance of an image segmentation technique. The dice scores for striatum segmentations are shown in Table 2. Our pixel accuracies are between 0.8–0.875, and are relatively high following [23]. The results of striatum segmentation of the patients are shown as Figs. 6–8.

Table 2: The dice scores of the patients.

Patient	Left-hand side	Right-hand side
1	0.825	0.870
2	0.883	0.810
3	0.870	0.875

Table 3: The L^2 error between actual data and numerical solution.

Patient	Right-hand side	Left-hand side
1	6.55%	6.36%
2	6.98%	5.79%
3	4.31%	5.77%
4	5.24%	5.15%

Numerical solution

Recall that our goal is to approximate the concentration of ^{18}F-FDOPA using the Diffusion equation (2) by means of the ADI method. Hence the two parameters α and β are needed to be determined in order to best fit our model with the true data. With respect to this, the pattern search method is used to improve the choice of α and β. The initial choice of the parameters of α and β are naturally chosen to be $\alpha = 1$ and $\beta = 1$ to normalize the diffusability in both directions. The same optimal parameters can also be reached by using other initial parameters. The uptake values of this radioactivity

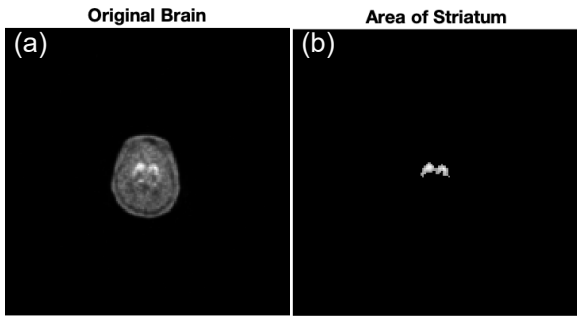

Fig. 6: Image segmentation of patient No. 1 by using Otsu's Algorithm with gray scale. (a) Original PET/CT imaging and (b) image segmentation of striatum.

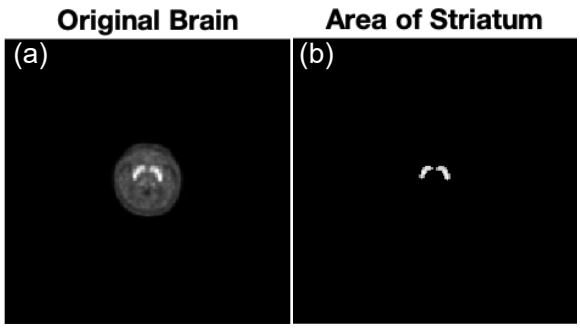

Fig. 7: Image segmentation of patient No. 2 by using Otsu's Algorithm with gray scale. (a) Original PET/CT imaging and (b) image segmentation of striatum.

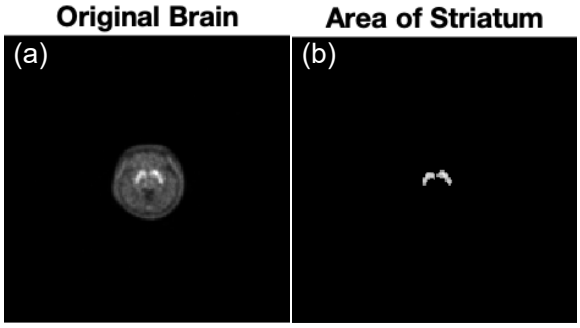

Fig. 8: Image segmentation of patient No. 3 by using Otsu's Algorithm with gray scale. (a) Original PET/CT imaging and (b) image segmentation of striatum.

were collected every 5 min since the patient get into PET/CT scan during 0 to 90 min after the injection. The initial time (t_0) is set at 15 min to imitate the fact that the brain tissue starts to absorb ^{18}F-FDOPA 15 min after the injection [24]. The concentration map of patients No.1–No.3 simulated by ADI method (Eq. (7)) are presented in Figs. 9–11. The numerical solution is then compared with the true data and the accuracy is presented in terms of the L_2 error (RMS), as can be seen in Table 3. Finally, we consider the average concentration of ^{18}F-FDOPA in the striatum at the initial and final time and compare the actual data with the numerical solution in the Table 4.

Table 4: Average concentration at the initial and final time.

Patient No.		Initial data (t_0)	Actual data ($t_{15} = 90$)	Numerical ($t_{15} = 90$)
1	Left striatum	8009.940	7529.076	7602.163
	Right striatum	8635.867	7669.282	7731.602
2	Left striatum	9635.571	11101.446	10806.775
	Right striatum	10082.866	10752.791	10643.788
3	Left striatum	12126.508	10749.044	10958.852
	Right striatum	12421.571	10018.326	10251.406

DISCUSSIONS AND REMARKS

The striatum area segmented by the Otsu's technique gives high pixel accuracy on which we can conveniently model the diffusion behavior and the numerical simulation of the concentration of FDOPA obtained. By applying the 2D ADI method on segmented region, we successfully approximate the concentration across the striatum at each time step with a reasonable overall accuracy no worse than 6.55%. The numerical solution of the concentration is also consistent with the patient profiles in all cases. One may see the variations in the concentration of ^{18}F-FDOPA in the striatum in Table 4. Notice the large decay in the final concentration of Patients No. 1 and No. 3 from both the actual and modelled data. On the contrary, note that the concentration in Patient No. 2 is quite static. This has confirmed that the numerical solutions from our model agree with the actual data and therefore lead to the same diagnosis of the possible PD.

Finally, we remark that this method can be used to interpolate the concentration in a more refined timescale or when some of the data is missing. It is also interesting to improve the model by imposing the behavior of the pharmaceutical substance as studied in [24]. In term of Clinical Pathology, this work can explain the decay of concentration at specific area. The results of this paper have the following advantages: (1) The proposed method is based on Otsu's segmentation technique which remove the unrelated effects outside the striatum area. (2) The simulation can be used to replace the missing or corrupted PET/CT scans. (3) The simulation can be used to interpolate the concentration of the radiopharmaceutical in the missing time. Finally, the proposed method can be futher extended to study the diffusion behavior of other radioactivity substances, for example ^{18}F-FDG which is used in cancer diagnosis.

Acknowledgements: The first author is financially supported by the Science Achievement Scholarship of Thailand and Department of Mathematics, Faculty of Science, King Mongkut's University of Technology Thonburi. Moreover, this research is supported by Thailand Science

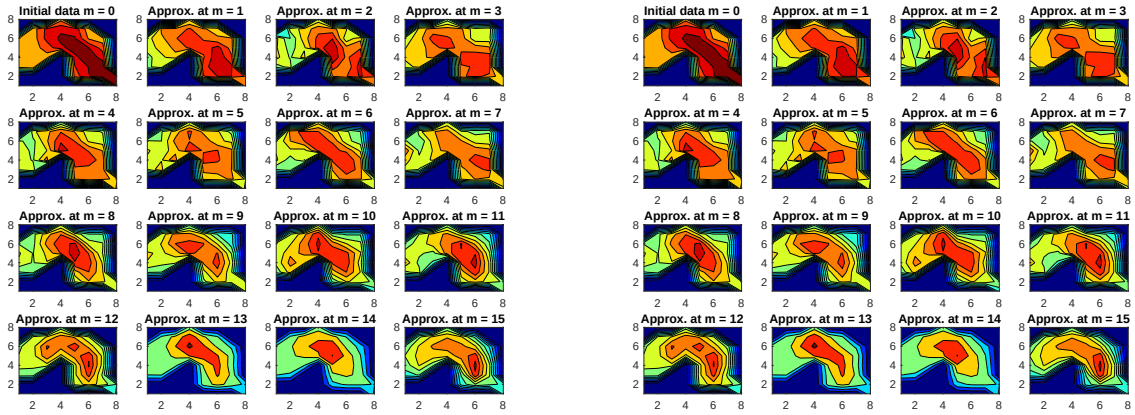

Fig. 9: Concentration map of patient No. 1 simulated by ADI method (Eq. (7)): (a) right striatum and (b) left striatum.

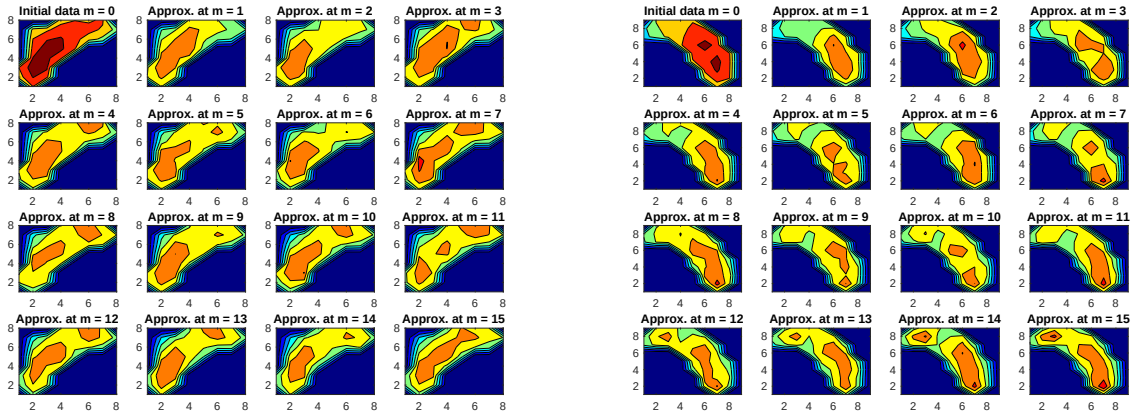

Fig. 10: Concentration map of patient No. 2 simulated by ADI method (Eq. (7)): (a) right striatum and (b) left striatum.

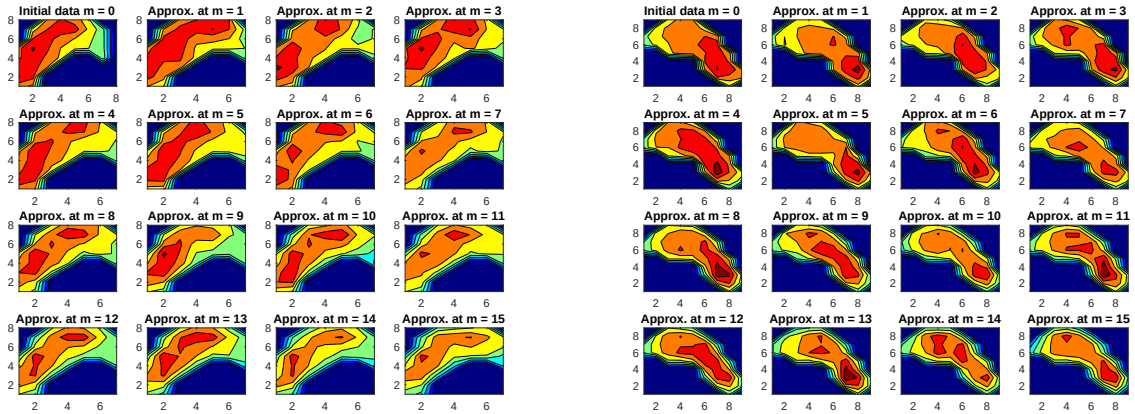

Fig. 11: Concentration map of patient No. 3 simulated by ADI method (Eq. (7)): (a) right striatum and (b) left striatum.

Research and Innovation (TSRI) Basic Research Fund: Fiscal year 2021 under project no. 64A306000005.

REFERENCES

1. Kish SJ, Tong J, Hornykiewicz O, Rajput A, Chang LJ, Guttman M, Furukawa Y (2008) Preferential loss of serotonin markers in caudate versus putamen in Parkinson's disease. *Brain* **131**, 120–131.
2. Pitcher TL, Melzer TR, MacAskill MR, Graham CF, Livingston L, Keenan RJ, Watts R, Dalrymple-Alford JC, et al (2012) Reduced striatal volumes in Parkinson's disease: a magnetic resonance imaging study. *Transl Neurodegener* **1**, ID 17.
3. Garg A, Appel-Cresswell S, Popuri K, McKeown MJ, Beg MF (2015) Morphological alterations in the caudate, putamen, pallidum, and thalamus in Parkinson's disease. *Front Neurosci* **9**, ID 101.
4. van Beilen M, Leenders KL (2006) Putamen FDOPA uptake and its relationship tot cognitive functioning in PD. *J Neurol Sci* **248**, 68–71.
5. Shalash AS, Hamid E, Elrassas HH, Bedair A, Abushouk AI, Khamis M, Hashim M, Ahmed N, et al (2018) Non-motor symptoms as predictors of quality of life in Egyptian patients with Parkinson's disease: A cross-sectional study using a culturally adapted 39-item Parkinson's disease questionnaire. *Front Neurol* **9**, ID 357.
6. Racette BA, Antenor JA, McGee-Minnich L, Moerlein SM, Videen TO, Kotagal V, Perlmutter JS (2005) [18F]FDOPA PET and clinical features in parkinsonism due to manganism. *Mov Disord* **20**, 492–496.
7. Broussolle E, Dentresangle C, Landais P, Garcia-Larrea L, Pollak P, Croisile B, Hibert O, Bonnefoi F, et al (1999) The relation of putamen and caudate nucleus 18F-Dopa uptake to motor and cognitive performances in Parkinson's disease. *J Neurol Sci* **166**, 141–151.
8. Chan LL, Rumpel H, Yap K, Lee E, Loo HV, Ho GL, Fook-Chong S, Yuen Y, et al (2007) Case control study of diffusion tensor imaging in Parkinson's disease. *J Neurol Neurosurg Psychiatry* **78**, 1383–1386.
9. Deep P, Gjedde A, Cumming P (1997) On the accuracy of an [18F]FDOPA compartmental model: evidence for vesicular storage of [18F]fluorodopamine *in vivo*. *J Neurosci Methods* **76**, 157–165.
10. Rakshi JS, Uema T, Ito K, Bailey D, Morrish P, Ashburner J, Dagher A, Jenkins I, et al (1999) Frontal, midbrain and striatal dopaminergic function in early and advanced Parkinson's disease A $_3$D [(18)F]dopa-PET study. *Brain* **122**, 1637–1650.
11. Nanni C, Fanti S, Rubello D (2007) ^{18}F-DOPA PET and PET/CT. *J Nucl Med* **48**, 1577–1579.
12. Keener J (1998) Biochemical reactions. In: Keener J, Sneyd J (eds) *Mathematical Physiology*, Springer-Verlag, New York, pp 1–47.
13. Fick A (1855) Ueber diffusion. *Ann Phys (Berl)* **170**, 59–86.
14. Goh TY, Basah SN, Yazid H, Safar MJA, Saad FSA (2018) Performance analysis of image thresholding: Otsu technique. *Measurement* **114**, 298–307.
15. Patlak CS, Hospod FE, Trowbridge SD, Newman GC (1998) Diffusion of radiotracers in normal and ischemic brain slices. *J Cereb Blood Flow Metab* **18**, 776–802.
16. Otsu N (1979) A threshold selection method from gray-level histograms. *IEEE Trans Syst Man Cybern Syst* **9**, 62–66.
17. Wray S (2016) Alternating direction implicit finite difference methods for the heat equation on general domains in two and three dimensions. PhD thesis, Colorado School of Mines, CO, USA.
18. Simoncini V (2016) Computational methods for linear matrix equations. *SIAM Rev* **58**, 377–441.
19. Rachford Jr DPH (1955) The numerical solution of parabolic and elliptic differential equations. *J Soc Indust Appl Math* **3**, 28–41.
20. Crank J, Nicolson P (1947) A practical method for numerical evaluation of solutions of partial differential equations of the heat-conduction type. In: *Mathematical Proceedings of the Cambridge Philosophical Society*, Cambridge Univ Press, Cambridge, pp 50–67.
21. Hooke R, Jeeves TA (1961) "direct search" solution of numerical and statistical problems. *J ACM* **8**, 212–229.
22. Davidon WC (1991) Variable metric method for minimization. *SIAM J Optim* **1**, 1–17.
23. Işın A, Direkoğlu C, Şah M (2016) Review of MRI-based brain tumor image segmentation using deep learning methods. *Procedia Comput Sci* **102**, 317–324.
24. Sanguansuttigul P, Saleewong T, Suksai S, Khamwan K, Bongsebandhu-phubhakdie S (2017) The kinetic model of 18 F-FDOPA in PET imaging correlated to brain structures : A case study on Parkinson' s disease. In: *Proceeding the 22nd Annual Meeting in Mathematics*, Chiang Mai, Thailand, pp 1–9.